THE JOURNAL OF PHYSICAL CHEMISTRY C

ARTICLE

pubs.acs.org/JPCC

Defects-Mediated Energy Transfer in Red-Light-Emitting Eu-Doped ZnO Nanowire Arrays

Dandan Wang,[†] Guozhong Xing,[†] Ming Gao,[‡] Lili Yang,[‡] Jinghai Yang,[‡] and Tom Wu*[,†]

[†]Division of Physics and Applied Physics, School of Physical and Mathematical Sciences, Nanyang Technological University, Singapore 637371

[‡]Institute of Condensed Matter Physics, Jilin Normal University, Siping, P. R. China 136000

ABSTRACT: We report on the photoluminescence in perfectly aligned Eu-doped ZnO nanowire arrays that are prepared on sapphire substrates using a vapor transport method with doped sol−gel precursor powder as the vapor source. Under the UV light excitation, Eu^{3+}-related red emission is observed in the Eu-doped ZnO nanowire arrays. By carrying out systematic temperature-dependent and time-resolved photoluminescence experiments, we identify a defect-mediated energy transfer pathway from the ZnO host to the Eu^{3+} ions. The energy transfer time increases from ∼9 to ∼130 ps after the nanowires are annealed in oxygen ambient, which reduces the defect concentration. This study suggests that defect engineering in bottom-up synthesis is a viable approach to modulate the energy transfer process, which may help to enable the future applications of ZnO-based nanomaterials in optoelectronics and full color displays.

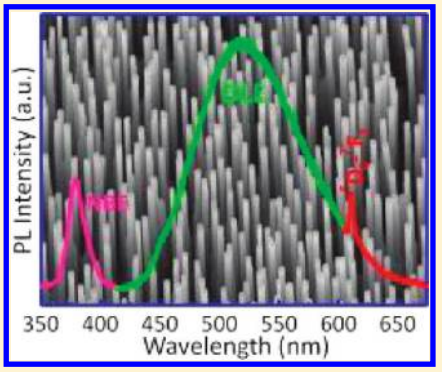

I. INTRODUCTION

Semiconductors doped with rare earth (RE) elements such as Eu, Er, Tm, and Tb have been intensively pursued because of their important applications in optoelectronics as emitters at visible wavelength.[1] There are two main factors leading to the stable and sharp luminescence in RE elements: one is that the 4f orbital of RE ions is shielded by the outer 6s, 5p, and 5d orbitals, which weakens its coupling with the surrounding ligands; the other is that the f−f transitions are parity forbidden, thus resulting in small absorption cross sections,[2] but the initial efforts of incorporating RE ions into Si and other narrow band gap semiconductors suffered severe limitations due to the solubility constraints and the thermal quenching.[3,4] Most recent studies have been focused on GaN to obtain efficient RE-based light emissions in the visible and infrared region.[5−9]

Like GaN, ZnO possesses the wurtzite structure and a wide band gap of 3.37 eV.[10,11] Furthermore, ZnO is low cost, environmental friendly, and shows high thermal and chemical stability. More importantly, ZnO has an exciton binding energy of 60 meV, which is much larger than the room-temperature (RT) thermal energy (25 meV).[12−14] Equipped with these unique properties, ZnO has been extensively exploited, in both the thin film and nanostructure forms, for potential optical and photonic applications.[15−19] There have been devices operating in green,[10] blue,[20] and near-UV[21] regions, but sharp red emission was rarely reported in ZnO. Can ZnO be doped with RE ions to emit red light? There have been recent efforts addressing this question by incorporating Eu as the RE activator to generate red light emission.[22−32] It was reported that Eu-doped ZnO exhibits the broadband luminescence in the visible spectral region at RT.[21,28−32] However, unlike GaN,[7,33,34] it is notoriously challenging to dope RE elements into ZnO because of the giant differences in ionic radius and charge. Even with confirmed doping, there was still no efficient light emission from the RE ions.[30] There are two main reasons leading to these disappointing results: One is that the luminescence lifetime of RE ions is at least 10^3 times longer than the excitons decay time in ZnO,[35,36] and this mismatch makes the direct energy transfer from ZnO to RE ions almost impossible; the other is the quenching effect on the RE emission due to the radiative transitions between the RE ions and the semiconductor host.[37]

To overcome the obstacles delineated above, several groups have suggested that defects, either intrinsic or extrinsic, can serve as the energy trapping centers to facilitate energy transfer and relevant light emission. Park et al. reported that extrinsic defects like chlorine impurities can assist the red emission in Eu^{3+}-doped ZnO.[29,31] In a more recent work, Zeng et al. suggested that in Eu-doped ZnO nanosheet-based microspheres Eu^{2+} ions act as the trapping centers and transfer energy to the Eu^{3+} ions, leading to the red emission.[32] Wang et al. indicated that the surface defects may act to help the process of energy transfer from ZnO to Eu^{3+} ions.[38] Despite these previous works, it remains an open question regarding the fast dynamics of energy transfer and how to optimize the red emission through defect engineering. The lack of qualitative study on the energy transfer process also severely hampers the development of this research. Furthermore, there are few reports on the vertically aligned 1D RE-doped ZnO nanowires (NWs) and their photoluminescence (PL) properties.

Received: May 17, 2011
Revised: October 9, 2011
Published: October 13, 2011

Herein, we report on the synthesis of vertical aligned Eu-doped ZnO NW arrays as well as the observation of red light emission under UV excitation, which can be attributed to the intra-4f transitions of Eu^{3+} ions. Moreover, our systematic studies using PL excitation, temperature-dependent PL, time-resolved PL (TRPL), and pump−probe transient absorption spectroscopy suggest that intrinsic defects, such as oxygen vacancies, mediate the energy transfer between the ZnO host to the Eu^{3+} ions. Furthermore, we qualitatively determined the energy transfer time to be ∼9 ps for the as grown Eu-doped ZnO NWs. Our results indicate that defects engineering is an effective approach to achieve the red emission in Eu-doped ZnO, which may help to exploit ZnO-based nanomaterials for photonics and full color display applications. This research also opens the door to investigating the energy transfer process in other doped wide band gap oxides.

II. EXPERIMENT DETAILS

Eu-doped ZnO NW arrays are synthesized on sapphire substrates using a two-step method comprising sol−gel precursor preparation and vapor transport growth. The source powder was obtained via a sol−gel method. $Zn(NO_3)_2 \cdot 6H_2O$ was dissolved in deionized water, then appropriate amounts of citric acid, ethylene glycol, and $Eu(NO_3)_3$ solution were added to the solution to a molar ratio of 0.97:0.03:3:12 for Zn/Eu/citric/ethylene glycol. The concentration of the metal ions in solution was adjusted to 0.01 M. The solution was stirred for 2 h until it became transparent and then was kept in the drying cabinet at 80 °C to form sol, which was then transformed into a gel at 130 °C. The solid resin was prepyrolyzed at 400 °C for 5 h to form Eu-doped ZnO composite powder. The experimental setup for the vapor transport growth has been previously described.[39−43] In brief, the precursor powder and graphite (99.99%, Aldrich) with a weight ratio of 1:1 were mixed and ground for 30 min before being introduced to the middle of a quartz tube in a horizontal furnace. Sapphire substrates with thin (1 to 2 nm) layers of Au were introduced to the quartz tube and placed a few centimeters downstream from the source. After the quartz tube was evacuated to a few milliTorrs (1 Torr = 1.333×10^2 Pa), the furnace was heated to 960 °C at a rate of 50 °C min^{-1}. The inner pressure was maintained at ∼25 Torr for a growth time of 15 min under a constant flow of 47.5 sccm Ar and 2.5 sccm O_2. After the furnace was cooled to room temperature, a light-gray layer was visible on the substrate surfaces. We named the as-grown sample EZO-1. To tailor the oxygen stoichiometry, we annealed sample at 600 °C under an oxygen atmosphere for 1 h, and the sample was named EZO-2. For comparison, we have also prepared undoped ZnO NW samples (UZO).

The crystal structure and morphology of the samples were studied by XRD (Bruker D8 advanced x-ray diffractometer), field-emission scanning electron microscopy (FESEM (JEOL JSM-6700 F, operated at 10 kV)), and transmission electron microscopy (TEM (JEOL 2100, operated at 200 kV)). A quantitative compositional analysis was carried out by using an X-ray photoelectron spectroscope (XPS (VG ESCALAB 220i-XL system equipped with a monochromatic X-ray source)) in an ultrahigh-vacuum chamber at a pressure $<1.0 \times 10^{-9}$ Torr. Peak positions are referenced to the adventitious C 1*s* peak taken to be 285.0 eV. For the room-temperature photoluminescence (RTPL) properties of the as-grown Eu-doped ZnO NWs, different wavelength laser was used as the excitation sources (λ_{exc} = 300, 325, 355, 440, and 488 nm). The excitation and emission spectra were taken on a Hitachi F-4500 spectrofluorimeter equipped with a 150 W xenon lamp as the excitation source at room temperature. Temperature dependent PL was measured with a 325 nm laser excitation between 5 and 300 K, and the data were collected by a CCD detector (Acton, Princeton Instruments PIXIS 400). To study the luminescence decay from the Eu-doped ZnO NWs, we used 325 nm, 150 fs excitation pulses (at a 1 kHz repetition rate) generated from an optical parametric amplifier (TOPAS) that was pumped using a regenerative amplifier (Coherent Legend) was used. The luminescence signal was dispersed by a DK240 1/4 m monochromator with 150 g/mm−500 nm grating and was time-resolved by an Optronis Streak Camera. The excitation average power was ∼10 μW. In the femtosecond transient transmission (i.e., pump−probe) measurements, the pump beam (325 nm) was used, and the probe beam (700 nm) was filtered from white light continuum.

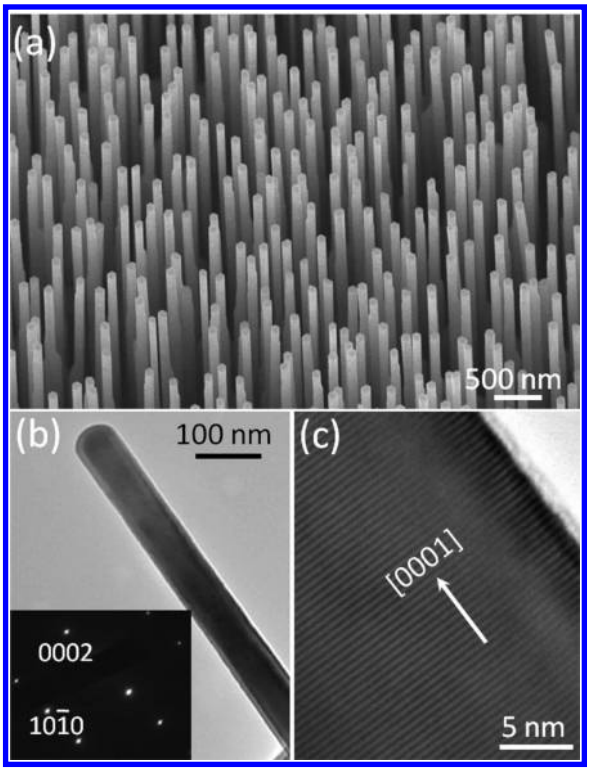

Figure 1. (a) FESEM image of as-grown Eu-doped ZnO nanowire arrays grown on a sapphire substrate. Representative (b) low- and (c) high-resolution TEM images of an individual Eu-doped ZnO nanowire and the corresponding SAED pattern (inset of panel b).

III. RESULTS AND DISCUSSION

A. Structural and Compositional Characterizations of Eu-Doped ZnO Nanowires. One main obstacle contributing to the ineffective Eu doping is the giant mismatch between the ion radius of Eu (0.095 nm) and Zn (0.060 nm). To tackle this problem, we developed a two-step vapor-based growth method, and we found that it is critical to prepare the doped precursor powder first by using a sol−gel method. The anion-rich environment inherent to the sol−gel route significantly benefits the doping process by suppressing the "self-purification" mechanism,[44] leading to the enhanced Eu doping. The properly doped precursor source ensures the simultaneous generation of Zn

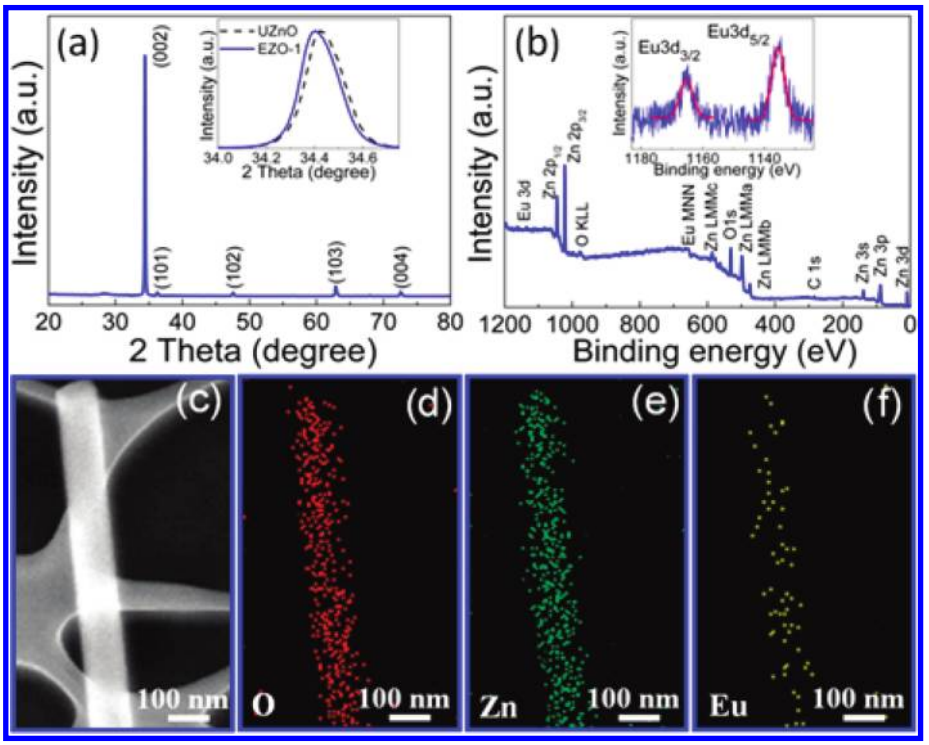

Figure 2. (a) XRD pattern of the Eu-doped ZnO NWs sample, EZO-1. Inset shows a shift of the (002) peak compared with the undoped ZnO sample. (b) XPS survey spectrum of EZO-1. Inset is the detail scan of the Eu $3d^{5/2}$ and $3d^{3/2}$ peaks. (c) FESEM image of an individual Eu-doped ZnO nanowire. (d−f) Corresponding EDS elemental mappings of O, Zn, and Eu.

and Eu vapors with the desired doping concentration. Our control experiments suggested that the correct stoichiometry could not be achieved in the grown products if a physically mixed power source was used. Furthermore, during the vapor transport growth the fine nanoparticles in the sol gel powder form intimate contact with the graphite to release effectively the metal vapor; indeed, no Eu doping was detected in the NWs if we simply mixed the source powder.

Figure 1a shows a FESEM image of the Eu-doped ZnO sample (EZO-1). The NW arrays are aligned perpendicular to the sapphire substrate as a result of the epitaxial growth. They exhibit diameters of 80−120 nm and lengths of 2 to 3 μm. The transmission electron microscopy (TEM) image in Figure 1b indicates that the surfaces of NW are smooth, and the rounded top ends may be solidified catalyst nanoparticles as a result of vapor−liquid−solid growth. The selected area electron diffraction (SAED) pattern in the inset suggests that the Eu-doped ZnO NWs can be indexed as the wurtzite ZnO structure with no detectable secondary phase. The high-resolution TEM image in Figure 1c shows that the NW has a crystallinity as good as the undoped ZnO NWs and grows along the [0001] direction; this high crystallinity also suggests that the Eu doping is uniform and does not introduce extensive defects.

In the XRD pattern of EZO-1 (Figure 2a), no impurity phase such as europium oxides was detected. As shown in the inset, the (002) peak shifts to a lower angle after doping due to the much larger radius of Eu^{3+} ions compared with that of Zn^{2+} ions. To investigate the chemical compositions and the bonding states, we performed XPS measurements. Prior to the XPS measurements, samples were cleaned by sputtering with an Ar ion beam to remove any potential surface contamination. A typical XPS survey scan obtained on EZO-1 is shown in Figure 2b. The survey scan confirms the presence of Zn, O, Eu, and C. As shown in the inset, the peaks at 1135.6 and 1165.2 eV correspond to Eu $3d_{5/2}$ and Eu $3d_{3/2}$, respectively,[45] and their positions indicate that the Eu ions have the +3 valence.[46] By fitting the integrated peak areas and applying the calibrated atomic sensitivity factors, the atomic percentages of Zn, O, and Eu in EZO-1 were calculated to be 56.8, 42.5, and 0.7, respectively. Therefore, EZO-1 has an Eu doping level of ∼1.2 at % and an oxygen deficiency of ∼26%. Previous theoretical calculations have suggested that the large oxygen deficiency in wide band gap oxides should be attributed to oxygen vacancies instead of cation interstitials,[47] which is particularly true if the growth takes place in an oxygen-poor environment. After postgrowth annealing in oxygen atmosphere, the oxygen deficiency dropped to ∼8.4% in EZO-2, whereas the valence state of Eu remained the same. From the XPS results alone, some surface segregation of Eu cannot be ruled out, but HRTEM, SAED, and XRD data suggest that the majority of Eu ions replace Zn in the ZnO matrix. Figure 2c is the FESEM image of an individual NW after being transferred to a copper grid. As shown in Figure 2d−f, the elemental mappings by using an energy-dispersive X-ray spectrometer (EDS) suggest that the distributions of Zn, O and Eu are quite homogeneous.

B. Photoluminescence Properties and Defects-Mediated Energy Transfer in Eu-Doped ZnO Nanowires. After confirming the Eu doping, we systemically investigated the optical properties of the undoped sample UZO, the as-grown Eu doped sample EZO-1, and the annealed sample EZO-2. Under 325 nm excitation, UZO exhibits a strong UV emission band centered at ∼380 nm (Figure 3a), which can be attributed to the near-band-edge (NBE) exciton recombination.[15] The broad defect-related green emission (GE) band centered at ∼510 nm has often been ascribed to the radiative recombination of photogenerated holes with electrons induced by the oxygen vacancies.[48,49] The origins of

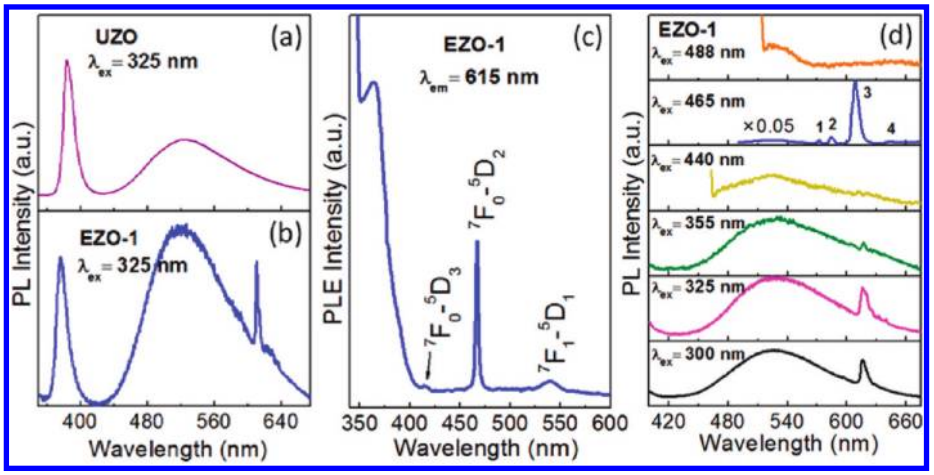

Figure 3. (a,b) Emission spectra of the undoped ZnO sample UZO and the Eu-doped ZnO sample EZO-1 under 325 nm excitation. (c) Excitation spectrum of EZO-1, monitored at 615 nm emission. (d) Emission spectra of EZO-1 under excitations of different wavelengths.

this GE band has been the subject of a long-standing controversy, and other sources such as V_{Zn} and donor−acceptor pair (DAP) recombination have also been proposed.[50] In contrast with the undoped sample UZO, an additional sharp red emission peak centering at ∼615 nm was observed in EZO-1 (Figure 3b). This peak can be attributed to the intra-4f transition of Eu^{3+} ions, in particular, the $^5D_0 \rightarrow {}^7F_2$ transition.[51] To understand the excitation process, we measured the excitation spectra monitored at 615 nm on sample EZO-1 in comparison with sample UZO. It should be noted that both the radiative defects and Eu ions can contribute to the 615 nm emission. As expected, in the excitation spectrum of UZO monitored at 615 nm emission, there is no resonant excitation at wavelength of ∼456 nm (not shown here), which allows us to deconvolve the emissions induced by the defects and the Eu ions. As shown in Figure 3c, in addition to the excitation peaks at 538, 467, 414, and 392 nm, which originate from the $^7F_1 \rightarrow {}^5D_1$, $^7F_0 \rightarrow {}^5D_J$ (J = 2, 3), and $^7F_0 \rightarrow {}^5L_6$ transitions of Eu^{3+} ions,[52,53] a strong excitation peak emerges in the UV regime, corresponding to the NBE transition in ZnO. The above-mentioned experimental results strongly suggest an energy transfer from the ZnO host to the Eu^{3+} ions.

The PL properties of EZO-1 under excitations of various wavelengths (300, 325, 355, 440, 465, and 488 nm) were also investigated, and the data are shown in Figure 3d. The 465 nm photon is resonant with the $^7F_0 \rightarrow {}^5D_2$ transition of the Eu^{3+} ions; the emission peaks 1− 4 under the resonant excitation can be assigned to the $^5D_0 \rightarrow {}^7F_J$ (J = 0, 1, 2, 3) transitions.[28] We also observed the red emission (615 nm) from the Eu^{3+} ions in the nonresonant excited spectra although the emission is much weaker than the resonant case. Such difference can be attributed to the fact that the resonant excitation directly excites the Eu^{3+} ions, therefore giving rise to a strong red emission with slow decay.[6] Under the UV excitation, only part of the Eu^{3+} ions can absorb energy from the host and the process energy transfer from the host is far less effective than the direct resonance absorption. Nevertheless, the observation of the red emission under the nonresonant conditions strongly suggests that there exists energy transfer mechanism between the ZnO host and the Eu^{3+} ions,[53,54] and below we will show that this energy transfer process is defect-mediated, most likely by oxygen vacancies.

The temperature-dependent PL measurements of the Eu-doped ZnO sample EZO-1 were also carried out under the 325 nm excitation (Figure 4a). The emissions around 370 (3.355 eV), 376 (3.30 eV), and 384 nm (3.23 eV) at low temperatures can be attributed to the donor-bound excitons (D^0X),[55] first- and second-order longitudinal optical phonon replica of free excitons (FX-1LO and FX-2LO),[10] respectively. At 5 and 50 K, in addition to the main defect emission band around 520 nm, a series of peaks appear at the higher-energy side, which is related to the strong electron-LO-phonon coupling.[56] The position of the red emission from the $^5D_0 \rightarrow {}^7F_2$ transition remains at 615 nm, showing no temperature dependence, as a result of the inner shell (intra-4f) nature of the transition.[1] In Figure 4b, we compare normalized integrated intensities of the Eu^{3+}-related red emission, the defect-related GE, and the exciton-related UV emission as a function of temperature. All of these emissions become progressively weaker with the increasing temperature due to the thermally activated nonradiative pathways.[57,58] The most notable feature is that the temperature-dependent evolution of the Eu^{3+}-related emission follows a similar trend as the defect emission but deviates from the exciton emission at high temperatures. This unambiguously indicates a strong correlation between the Eu^{3+}-related red emission with the defects, and these defects (oxygen vacancies) can function as energy storage centers that mediate the energy transfer from the ZnO host to the Eu^{3+} ions. Therefore, the correlation between the Eu^{3+}-related red emission and the defect emission is a "positive" one, exhibiting similar temperature dependence.

To investigate this correlation further, we carried out some comparative measurements on the as-grown Eu-doped ZnO (EZO-1) and the annealed Eu-doped ZnO (EZO-2) samples. Figure 5a shows the normalized emission spectra of EZO-1 and EZO-2 under the excitation at 325 nm. After annealing, both the defect-related GE and the Eu^{3+}-related red emission are considerably quenched. Importantly, the decrease in the red emission is correlated to a corresponding decrease in oxygen deficiency from ∼26% in EZO-1 to ∼8.4% in EZO-2. This further supports our hypothesis that oxygen vacancies facilitate the energy transfer process. Considering the previous examples of RE activators in II−VI semiconductors[32,59] and the results of self-interaction corrected local spin density method,[60] we propose the energy transfer mechanism, as illustrated in Figure 6. Following above bandgap excitation, the carriers relax to the band edge of the conduction band (CB) and valence band (VB), where they are rapidly trapped at the defects or undergo subsequent band edge

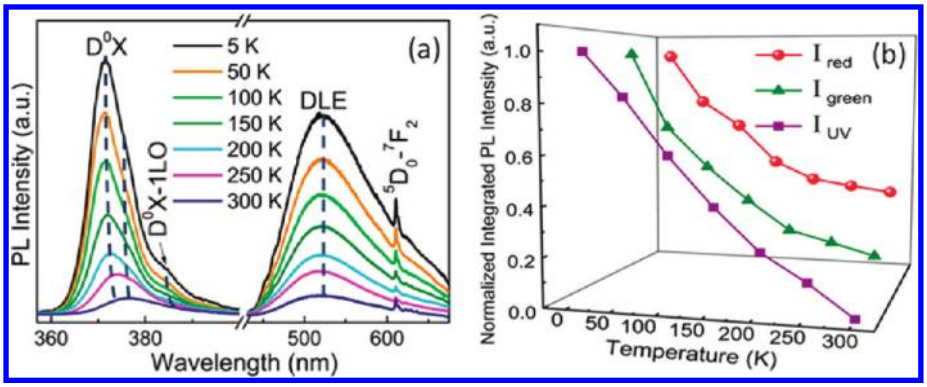

Figure 4. (a) Temperature-dependent photoluminescence spectra of the Eu-doped ZnO nanowire sample EZO-1 under excitation at 325 nm. (b) Temperature dependences of the integrated intensities of the red, green, and UV emissions.

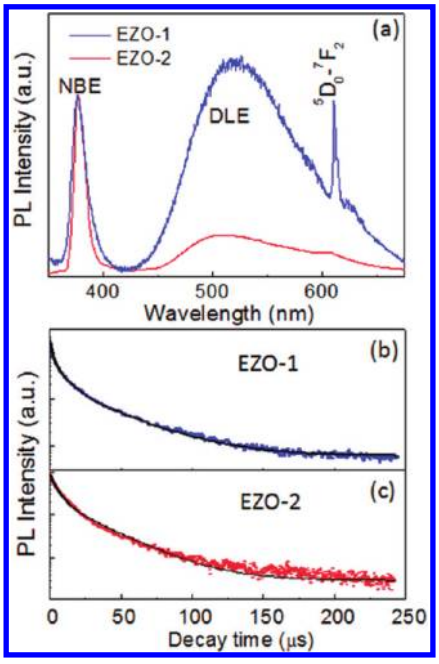

Figure 5. (a) Emission spectra of the as-grown sample EZO-1 and the annealed sample EZO-2 under excitation at 325 nm. (b,c) Time decay of luminescence in EZO-1 and EZO-2 for the 615 nm emission under excitation at 325 nm; dots are the experiment date and black lines are the exponential fitting results.

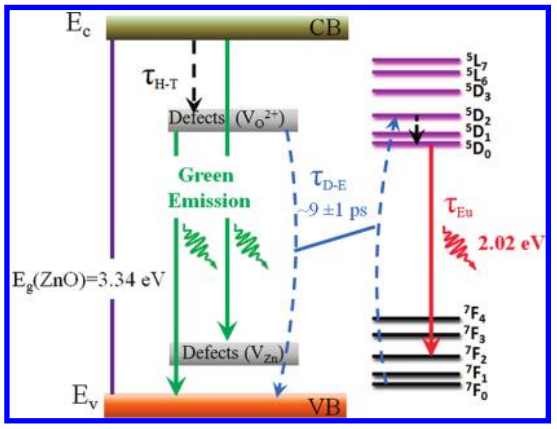

Figure 6. Schematic illustrating the proposed mechanism of energy transfer from the ZnO host to the Eu^{3+} ions. The dashed and the solid lines represent nonradiative and radiative processes, respectively. The green emission may be multiorigin in nature, and some of the possible radiative pathways are also indicated.

radiative emission. By means of a resonant energy transfer (RET) process, as shown in Figure 6, the trapped carriers at the oxygen vacancies could transfer their energy to the Eu^{3+} subsystem (i.e., $^7F_0 \rightarrow {}^5D_2$). As a final step of the energetic process, Eu^{3+} ions go through the radiative transition from $^5D_0$ to $^7F_2$, giving out the red emission. The TRPL data shown in Figures 5b,c were fitted using a biexponential decay function $A_1 \exp(-t/\tau_1) + A_2 \exp(-t/\tau_2)$, where the decay lifetimes were determined to be $\tau_1 = 33.4 \pm 0.6$ ($\tau_2 = 7.2 \pm 0.1$) μs and $\tau_1 = 40.1 \pm 1.02$ ($\tau_2 = 9.8 \pm 0.09$) μs for sample EZO-1 and EZO-2, respectively. The fast decay component (τ_2) most likely originates from the nonradiative recombination process at room temperature.[12] The slow decay component (τ_1) in EZO-1 (33.4 μs) is smaller than that in EZO-2 (40.1 μs). This difference indicates that annealing significantly reduces the defect states and weakens the energy transfer, similar to the previous report on Er^{3+}/GaN.[61]

To gain a deeper insight into the time scales of the energy transfer between the ZnO host and the Eu subsystem, we conducted femtosecond transient transmission measurements at low pump intensity (~0.2 GW/cm^2), and the results are shown in Figure 7a,b. Probing with an energy of 1.77 eV (700 nm), which is significantly less than the bandgap of ZnO, will allow us to interrogate the carrier populations at the band edges and the defect states through monitoring the photoabsorption (PA) of these carriers to the excited states (i.e., a decreased transmittance of the probe). Depopulation of the band edge carriers could arise from a few possibilities: (a) radiative or nonradiative recombination, (b) multiphonon emission, and (c) fast trapping of carriers to the defect states. Depopulation of the carriers trapped at the defect states could arise from (a), (b), and (d) RET to the Eu subsystem. This will manifest as a decay of the PA signals to the equilibrium in the differential transmittance (DT) profiles, as shown in Figures 7a,b. There is notable difference in the PA signals between the Eu-doped ZnO and the undoped ZnO samples in the first few hundred picoseconds, indicating a fast energy transfer between the ZnO host and the Eu ions in the doped samples. The PA signals follow very similar decay trends after 300 ps, suggesting the same PA decay process for both the undoped and Eu-doped ZnO NWs in the long time range. Therefore, the pump probe data were normalized

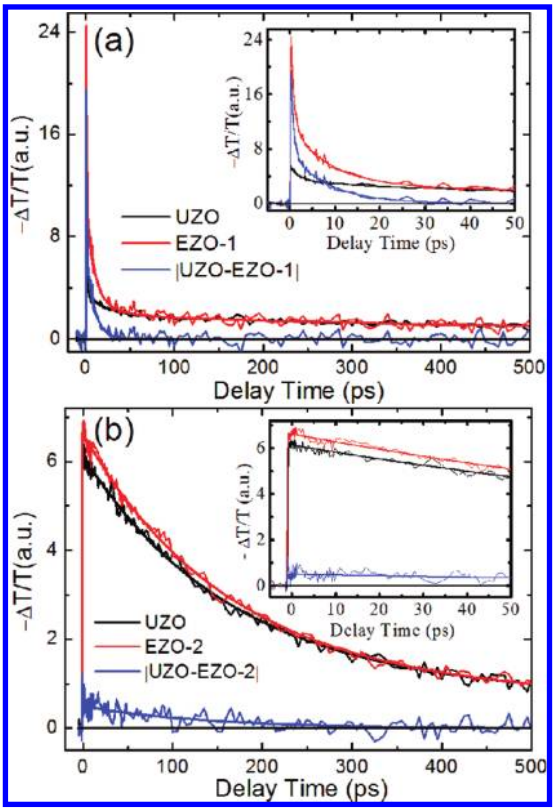

Figure 7. (a) Normalized transient absorption data obtained with 310 nm pump and 700 nm probe and fitting to exponential functions in the as-grown undoped (black) and Eu-doped (red) ZnO NW samples. The blue curve shows the difference between the two. (b) Corresponding data after the Eu-doped ZnO sample were annealed under an oxygen atmosphere. Insets show the decay dynamics in the range of 0−50 ps.

according to the level of the long tail (500 ps), and afterward the energy transfer time between the ZnO and the Eu ions was extracted.

From the carrier dynamics in the Eu-doped and undoped ZnO, the energy transfer time $\tau_{D\text{-}E}$ from the ZnO to the Eu^{3+} ions can be obtained through a "subtractive" procedure similar to that used to study Mn-doped CdS/ZnS core/shell nanoparticles.[62] In Figure 7a, within the initial 40 ps, the Eu-doped ZnO sample EZO-1 decays much faster than the undoped sample UZO, which we attribute to the energy transfer from the ZnO host to the Eu^{3+} ions.[62] We took the difference of the decay data, and through fitting to the exponential decay, we obtained an energy transfer time of $\sim 9 \pm 1$ ps, which indicts a very fast energy transfer process. Furthermore, we also examined the carrier relaxation dynamics in the undoped ZnO and the Eu-doped samples after annealing in oxygen atmosphere. The carrier decay dynamics in EZO-2 show a very similar trend like the undoped sample (Figure 7b), but a much longer energy transfer time of $\sim 130 \pm 4$ ps was obtained. The reduced population of defects in the annealed sample makes the energy transfer to the Eu subsystem less efficient. This strongly supports our hypothesis that the intrinsic defects can effectively assist the energy transfer.

In general, transfer of the excitation energy from the host to the doping ions is rather inefficient, and most of the energy is released through other channels, such as multiple phonon nonradiative transitions, bound excitons, and self-activated centers.[63] However, if one produces certain defects in the host as trapping and energy storage centers, then energy transfer can be much enhanced.[64] The effective spectral overlap of the emission from the defects and the absorption of the Eu^{3+} ions enables the ultrafast energy transfer through a resonant energy transfer process. It can also be envisaged that more effective energy transfer pathways could be realized in the future via appropriate defect engineering and tuning the majority of defects to participate actively in the energy transfer process, which will eventually gives more intense RE ions-related emissions.

IV. CONCLUSIONS

In summary, we have developed a two-step method to dope efficiently Eu into aligned ZnO NW arrays grown on sapphire substrates, which involves the preparation of doped sol−gel precursor and the NW growth via vapor transport. We observed the UV-excited red emission of the Eu^{3+} ions at room temperature in the aligned NW arrays. Furthermore, we found evidence of a defect-mediated resonant energy transfer process between the ZnO host and the Eu subsystem. The ultrafast dynamics of the energy transfer process was also corroborated by the femtosecond transient transmission measurements where an energy transfer time of 9 ± 1 ps was measured for the as grown Eu-doped ZnO NWs. The energy transfer time could be tailored from ∼9 to ∼130 ps by reducing the defect concentration through annealing the NWs in oxygen atmosphere. Overall, to achieve effective light emission in doped ZnO, it is of paramount important that the appropriate energy transfer process is established and a high percentage of the engineered defects can effectively participate in this process. The present study suggests that via defect engineering, rare-earth-doped ZnO NWs have the potential to give efficient multicolor emissions and may find applications in optoelectronic and display devices.

AUTHOR INFORMATION

Corresponding Author

*Tel: (65) 6514 1047. Fax: (65) 6794 1325 E-mail: tomwu@ntu.edu.sg.

ACKNOWLEDGMENT

This work was partially supported by the Singapore National Research Foundation. G.Z.X. acknowledges the financial support of Singapore Millennium Foundation Scholarship. We also thank T. C. Sum, G. C. Xing, and A. C. H. Huan for valuable discussion and experimental assistants. D. D. Wang and G. Z. Xing contributed equally to this work.

REFERENCES

(1) Steckl, J.; Park, J. H.; Zavada, J. M. *Mater. Today* **2007**, *10*, 20.
(2) Godlewski, M.; Leskelä, M. *Crit. Rev. Solid State Mater. Sci.* **1994**, *19*, 199.
(3) Ennen, H.; Schneider, J.; Pomrenke, G.; Axmann, A. *Appl. Phys. Lett.* **1983**, *43*, 943.
(4) Ennen, H.; Pomrenke, G.; Axmann, A.; Eisele, K.; Haydl, W.; Schneider, J. *Appl. Phys. Lett.* **1985**, *46*, 381.
(5) Park, J. H.; Steckl, A. J. *J. Appl. Phys.* **2005**, *98*, 56108.
(6) Peng, H. Y.; Lee, C. W.; Everitt, H. O.; Lee, D. S.; Steckl, A. J.; Zavada, J. M. *Appl. Phys. Lett.* **2005**, *86*, 51110.
(7) Wang, K.; Martin, R. W.; O'Donnell, K. P.; Katchkanov, V.; Nogales, E.; Lorenz, K.; Alves, E.; Ruffenach, S.; Briot, O. *Appl. Phys. Lett.* **2005**, *87*, 112107.

(8) Nyein, E. E.; Hommerich, U.; Heikenfeld, J.; Lee, D. S.; Steckl, A. J.; Zavada, J. M. *Appl. Phys. Lett.* **2003**, *82*, 1655.
(9) Bodiou, L.; Braud, A.; Doualan, J. L.; Moncorge, R.; Park, J. H.; Munasinghe, C.; Steckl, A. J.; Lorenz, K.; Alves, E.; Daudin, B. *J. Appl. Phys.* **2009**, *105*, 043104.
(10) Özgür, Ü.; Alivov, Y. I.; Liu, C.; Teke, A.; Reshchikov, M. A.; Dogan, S.; Avrutin, V.; Cho, S. J.; Morko, H. *J. Appl. Phys.* **2005**, *98*, 041301.
(11) Klingshirn, C. *Chemphyschem* **2007**, *8*, 782.
(12) Yang, J. H.; Wang, D. D.; Yang, L. L.; Zhang, Y. J.; Xing, G. Z.; Lang, J. H.; Fan, H. G.; Gao, M.; Wang, Y. X. *J. Alloys Comp.* **2008**, *450*, 508.
(13) Fang, X. S.; Ye, C. H.; Zhang, L. D.; Li, Y.; Xiao, Z. D. *Chem. Lett.* **2005**, *34*, 436.
(14) Fang, X. S.; Bando, Y.; Gautam, U. K.; Zhai, T. Y.; Zeng, H. B.; Xu, X. J.; Liao, M. Y.; Golberg, D. *Crit. Rev. Solid* **2009**, *34*, 190.
(15) Djurišić, A. B.; Leung, Y. H. *Small* **2006**, *2*, 944.
(16) Cui, J. B.; Gibson, U. *Nanotechnology* **2007**, *18*, 155302.
(17) Chen, T.; Xing, G. Z.; Zhang, Z.; Chen, H. Y.; Wu, T. *Nanotechnology* **2008**, *19*, 435711.
(18) Liu, K. W.; Chen, R.; Xing, G. Z.; Wu, T.; Sun, H. D. *Appl. Phys. Lett.* **2010**, *96*, 023111.
(19) Wang, D. D.; Yang, J. H.; Xing, G. Z.; Yang, L. L.; Lang, J. H.; Gao, M.; Yao, B.; Wu, T. *J. Lumin.* **2009**, *129*, 996.
(20) Zhang, X. M.; Lu, M. Y.; Zhang, Y.; Chen, L. J.; Wang, Z. L. *Adv. Mater.* **2009**, *21*, 2767.
(21) Huang, M. H.; Mao, S.; Feick, H.; Yan, H. Q.; Wu, Y. Y.; Kind, H.; Weber, E.; Russo, R.; Yang, P. D. *Science* **2001**, *292*, 1897.
(22) Gao, S.; Zhang, H.; Deng, R.; Wang, X.; Sun, D.; Zheng, G. *Appl. Phys. Lett.* **2008**, *89*, 123125.
(23) Armelao, L.; Heigl, F.; Ju1rgensen, A.; Blyth, R. I. R.; Regier, T.; Zhou, X.-T.; Sham, T. K. *J. Phys. Chem. C* **2007**, *111*, 10194.
(24) Liu, Y. S.; Luo, W.; Li, R.; Liu, G.; Antonio, R. M.; Chen, X. *J. Phys. Chem. C* **2008**, *112*, 686.
(25) Pauporte, T.; Pelle, F.; Viana, B.; Aschehoug, P. *J. Phys. Chem. C* **2007**, *111*, 15427.
(26) Armelao, L.; Bottaro, G.; Pascolini, M.; Sessolo, M.; Tondello, E.; Bettinelli, M.; Speghini, A. *J. Phys. Chem. C* **2008**, *112*, 4049.
(27) Liu, Y.; Luo, W.; Li, R.; Chen, X. *Opt. Lett.* **2007**, *32*, 566.
(28) Du, Y. P.; Zhang, Y. W.; Sun, L. D.; Yan, C. H. *J. Phys. Chem. C* **2008**, *112*, 12234.
(29) Park, Y. K.; Han, J. I.; Kwak, M. G.; Yang, H.; Ju, S. H.; Cho, W. S. *Appl. Phys. Lett.* **1998**, *72*, 668.
(30) Hayashi, Y.; Narahara, H.; Uchida, T.; Noguchi, T.; Ibuki, S. *Jpn. J. Appl. Phys.* **1995**, *34*, 1878.
(31) Park, Y. K.; Han, J. I.; Kwak, M. G.; Yang, H.; Sung Hoo, J.; Cho, W. S. *J. Lumin.* **1998**, *78*, 87.
(32) Zeng, X. Y.; Yuan, J. L.; Wang, Z. Y.; Zhang, L. *Adv. Mater.* **2007**, *19*, 4510.
(33) Andreev, T.; Monroy, E.; Gayral, B.; Daudin, B.; Liem, N. Q.; Hori, Y.; Tanaka, M.; Oda, O.; Dang, D. L. S. *Appl. Phys. Lett.* **2005**, *87*, 021906.
(34) Wang, R.; Steckl, A. J.; Brown, E. E.; Hommerich, U.; Zavada, J. M. *J. Appl. Phys.* **2009**, *105*, 043107.
(35) Yolanda, C.; Beatriz, J.; Cedric, B.; Bruno, V.; Heinz, A.; David, G.; Clement, S. *Nanotechnology* **2007**, *18*, 055705.
(36) Lee, S.-K.; Chen, S. L.; Hongxing, D.; Sun, L.; Chen, Z.; Chen, W. M.; Buyanova, I. A. *Appl. Phys. Lett.* **2010**, *96*, 083104.
(37) Quang, V. X.; Liem, N. Q.; Thana, N. C.; Chuong, T. V.; Thanh, L. T. L. *Phys. Status Solidi A* **1983**, *78*, K161.
(38) Wang, M.; Huang, C.; Huang, Z.; Guo, W.; Huang, J.; He, H.; Wang, H.; Cao, Y.; Liu, Q.; Liang, J. *Opt. Mater.* **2009**, *31*, 1502.
(39) Xing, G. Z.; Yi, J. B.; Wang, D. D.; Liao, L.; Yu, T.; Shen, Z. X.; Huan, C. H. A.; Sum, T. C.; Ding, J.; Wu, T. *Phys. Rev. B* **2009**, *79*, 174406.
(40) Wang, D. D.; Xing, G. Z.; Peng, H. Y.; Wu, T. *J. Phys. Chem. C* **2009**, *113*, 7065.
(41) Xing, G. Z.; Zhang, Z.; Wang, D. D.; Fang, X. S.; Huang, X.; Guo, J.; Liao, L.; Zheng, Z.; Xu, H. R.; Yu, T.; Shen, Z. X.; Huan, C. H. A.; Sum, T. C.; Zhang, H.; Wu, T. *Nanotechnology* **2010**, *21*, 255701.
(42) Xing, G. Z.; Yi, J. B.; Tao, J. G.; Liu, T.; Wong, L. M.; Zhang, Z.; Li, G. P.; Wang, S. J.; Ding, J.; Sum, T. C.; Huan, C. H. A.; Wu, T. *Adv. Mater.* **2008**, *20*, 3521.
(43) Zhang, Z.; Wong, L. M.; Ong, H. G.; Wang, X. J.; Wang, J. L.; Wang, S. J.; Chen, H. Y.; Wu, T. *Nano Lett.* **2008**, *8*, 3205.
(44) Gustavo, M. D.; James, R. C. *Phys. Rev. Lett.* **2006**, *96*, 226802.
(45) Tan, X. L.; Wang, X. K.; Geckeis, H.; Rabung, T. H. *Environ. Sci. Technol.* **2008**, *42*, 6532.
(46) Vercaemst, R.; Poelman, D.; Fiermans, L.; Van Meirhaeghe, R. L.; Laflere, W. H.; Cardon, F. *J. Electron Spectrosc., Relat. Phenom.* **1995**, *74*, 45.
(47) Stephan, L.; Alex, Z. *Phys. Rev. Lett.* **2007**, *98*, 045501.
(48) Tay, Y. Y.; Tan, T. T.; Boey, F.; Liang, M. H.; Ye, J.; Zhao, Y.; Norby, T.; Li, S. *Phys. Chem. Chem. Phys.* **2010**, *12*, 2373.
(49) Dileep, K.; Panchakarla, L. S.; Balasubramanian, K.; Waghmare, U. V.; Datta, R. *J. Appl. Phys.* **2011**, *109*, 063523.
(50) Armelao, L.; Heigl, F.; Brunet, S.; Sammynaiken, R.; Regier, T.; Blyth, R. I. R.; Zuin, L.; Sankari, R.; Vogt, J.; Sham, T.-K. *ChemPhysChem* **2010**, *11*, 3625.
(51) Zeng, X. Y.; Yuan, J. L.; Zhang, L. D. *J. Phys. Chem. C* **2008**, *112*, 3503.
(52) Dejneka, M.; Snitzer, E.; Riman, R. E. *J. Lumin.* **1995**, *65*, 227.
(53) Ebisawa, K.; Okuno, T.; Abe, K. *Jpn. J. Appl. Phys.* **2008**, *47*, 7236.
(54) Atsushi, I.; Yoshihiko, K. *Appl. Phys. Lett.* **2005**, *86*, 253106.
(55) Al-Suleiman, M.; Mofor, A. C.; El-Shaer, A.; Bakin, A.; Wehmann, H. H.; Waag, A. *Appl. Phys. Lett.* **2006**, *89*, 231911.
(56) Woong-Ki, H.; Gunho, J.; Minhyeok, C.; Takhee, L.; Jung Inn, S.; Mark, E. W. *Appl. Phys. Lett.* **2009**, *94*, 043103.
(57) Van Dijken, A.; Meulenkamp, E. A.; Vanmaekelbergh, D.; Meijerink, A. *J. Phys. Chem. B* **2000**, *104*, 1715.
(58) Ye, H. B.; Kong, J. F.; Shen, W. Z.; Zhao, J. L.; Li, X. M. *J. Phys. D: Appl. Phys.* **2007**, *40*, 5588.
(59) Lathika Devi, S. K.; Sudarsana Kumar, K.; Balakrishnan, A. *Mater. Lett.* **2011**, *65*, 35.
(60) Svane, A.; Christensen, N. E.; Petit, L.; Szotek, Z.; Temmerman, W. M. *Phys. Rev. B* **2006**, *74*, 165204.
(61) Bodiou, L.; Braud, A. *Appl. Phys. Lett.* **2008**, *93*, 151107.
(62) Chen, H.-Y.; Chen, T.-Y.; Son, D. H. *J. Phys. Chem. C* **2010**, *114*, 4418.
(63) Jia, W. Y.; Monge, K.; Fernandez, F. *Opt. Mater.* **2003**, *23*, 27.
(64) Prezzi, D.; Eberlein, T. A. G.; Filhol, J. S.; Jones, R.; Shaw, M. J.; Briddon, P. R.; Oberg, S. *Phys. Rev. B* **2004**, *69*, 193202.